






Companions to *Kepler* giant stars: A long-period eccentric sub-stellar companion to KIC 3526061 and a stellar companion to HD 187878[★]

Marie Karjalainen¹[★], Raine Karjalainen¹[★], Artie P. Hatzes², Holger Lehmann², Pierre Kervella³, Saskia Hekker^{4,5,6}, Hans Van Winckel⁷, Jakub Überlauer⁸, Michaela Vítková⁹, Marek Skarka^{1,9}, Petr Kabáth¹, Saskia Prins⁷, Andrew Tkachenko⁷, William D. Cochran¹⁰, and Alain Jorissen¹¹

¹ Astronomical Institute, Czech Academy of Sciences, 251 65 Ondřejov, Czech Republic
e-mail: marie.karjalainen@asu.cas.cz

² Thüringer Landessternwarte Tautenburg, Sternwarte 5, Tautenburg 07778, Germany

³ LESIA, Observatoire de Paris, Université PSL, CNRS, Sorbonne Université, Univ. Paris Diderot, Sorbonne Paris Cité, 5 place Jules Janssen, 92195 Meudon, France

⁴ Max-Planck-Institut für Sonnensystemforschung, Justus-von-Liebig-Weg 3, Göttingen 37077, Germany

⁵ Center for Astronomy (ZAH/LSW), Heidelberg University, Königstuhl 12, 69117 Heidelberg, Germany

⁶ Heidelberg Institute for Theoretical Studies (HITS) gGmbH, Schloss-Wolfsbrunnengasse 35, 69118 Heidelberg, Germany

⁷ Instituut voor Sterrenkunde, KU Leuven, Celestijnenlaan 200D bus 2401, Leuven 3001, Belgium

⁸ Astronomical Institute, Faculty of Mathematics and Physics, Charles University, V Holešovičkách 2, 18000 Praha 8, Czech Republic

⁹ Department of Theoretical Physics and Astrophysics, Masaryk University, Kotlářská 2, 61137 Brno, Czech Republic

¹⁰ McDonald Observatory and Center for Planetary Systems Habitability, The University of Texas, Austin, Texas, USA

¹¹ Institut d'Astronomie et d'Astrophysique, Université Libre de Bruxelles C.P. 226, Boulevard du Triomphe, 1050 Bruxelles, Belgium

Received 14 July 2022 / Accepted 19 September 2022

ABSTRACT

Context. Our knowledge of populations and the occurrence of planets orbiting evolved intermediate-mass stars is still incomplete. In 2010 we started a planet search programme among 95 giant stars observed by the *Kepler* mission to increase the sample of giant stars with planets and with reliable estimates of stellar masses and radii.

Aims. We present the two systems from our planet search programme whose companions we were able to characterise: KIC 3526061 and HD 187878.

Methods. We used precise stellar radial velocity measurements taken with four different echelle spectrographs to derive an orbital solution. We used *Gaia* astrometric measurements to obtain the inclination of the HD 187878 system and *Kepler* photometric observations to estimate the stellar mass and radius.

Results. We report the discovery of a sub-stellar companion and a stellar companion around two intermediate-mass red giant branch stars. KIC 3526061 b is most likely a brown dwarf with a minimum mass of $18.15 \pm 0.44 M_{\text{Jupiter}}$ in a long-period eccentric orbit, with orbital period 3552^{+158}_{-135} d and orbital eccentricity $e = 0.85 \pm 0.01$. It is the most evolved system found having a sub-stellar companion with such a high eccentricity and wide separation. HD 187878 B has a minimum mass of $78.4 \pm 2.0 M_{\text{Jupiter}}$. Combining the spectroscopic orbital parameters with the astrometric proper motion anomaly, we derived an orbital inclination $i = 9.8^{+0.4}_{-0.6}$ deg, which corresponds to the companion's mass in the stellar regime of $0.51^{+0.04}_{-0.02} M_{\odot}$.

Conclusions. A sub-stellar companion of KIC 3526061 extends the sample of known red giant branch stars with sub-stellar companions on very eccentric wide orbits, and might provide a probe of the dynamical evolution of such systems over time.

Key words. methods: observational – techniques: radial velocities – techniques: spectroscopic – stars: individual: KIC 3526061 – stars: individual: HD 187878 – brown dwarfs

1. Introduction

The two most successful techniques for the detection of exoplanets are the transit method and the Doppler method, and both are biased towards host stars with masses less than $\sim 1 M_{\odot}$. Detecting transit signals due to planets for intermediate-mass stars ($1.2\text{--}2 M_{\odot}$) is more difficult than for lower-mass dwarf stars,

due to the larger stellar radius of more massive stars. Likewise, intermediate-mass main sequence stars are ill-suited for the radial velocity (RV) method. They are hot, and thus have few spectral lines for the RV measurement. More problematic, the stars have appreciable amounts of rotation that broadens the spectral lines and makes them more shallow, which further decreases the RV precision and makes the detection of planetary companions difficult.

On the other hand, intermediate-mass stars that have evolved to giant stars are cool so they have more spectral lines and usually rotate slowly, which means that the spectral lines are

* Full Tables 1 and 2 are only available at the CDS via anonymous ftp to cdsarc.cds.unistra.fr (130.79.128.5) or via <https://cdsarc.cds.unistra.fr/viz-bin/cat/J/A+A/668/A26>

** These authors contributed equally to this work.

narrower. One can easily obtain an RV precision of several m s^{-1} on a $2 M_{\odot}$ giant star compared to tens of m s^{-1} for its main sequence progenitor. The giant stars thus serve as proxies for planet searches around intermediate-mass early-type main sequence stars.

Since the discovery of the first exoplanets around K-giant stars (Hatzes & Cochran 1993; Frink et al. 2002), several teams have been surveying the so-called retired A stars using the RV method, with the goal of learning more about the occurrence and properties of planets around more massive stars. These surveys discovered most of the over 150 exoplanets orbiting giant stars, which is 3% of the total exoplanets known to date¹. Our list of exoplanets orbiting giant stars excludes those orbiting subgiants, and includes companions with a mass or minimum mass of $< 13 M_{\text{Jupiter}}$.

Studying extrasolar planets around K-giant stars is essential to determine the planetary occurrence versus the stellar mass and metallicity, which in turn is important to better understand the planet formation and evolution processes. The disk instability model predicts that there should be no dependence of stellar host mass on planet formation and physical stellar properties (Boss 2006). On the other hand, the core-accretion formation process, which is believed to be at the origin of most of the planets, predicts an increase in giant planet frequency with stellar mass up to $3 M_{\odot}$ (Kennedy & Kenyon 2008). Most studies confirm the trend of the higher giant planet occurrence for higher stellar host masses (for example Bowler et al. 2010; Johnson et al. 2010; Reffert et al. 2015; Jones et al. 2016; Ghezzi et al. 2018), which provides an additional support for the core accretion mechanism of planet formation. However, unlike for a main sequence star, it is more problematic to determine the stellar mass of a giant star. Evolutionary tracks for stars covering a wide range of masses all converge to a similar region of the H-R diagram.

Fortunately, the stellar mass can be derived from solar-like oscillations that are ubiquitous in K-giant stars. Their first firm discovery in a giant star was made by Frandsen et al. (2002). However, only later were they unambiguously found in late-type giant stars, thanks to the CoRoT (De Ridder et al. 2009) and the *Kepler* (Huber et al. 2010; Kallinger et al. 2010) space missions. The *Kepler* mission was monitoring a sample of over 13 000 red giant stars that can be used for asteroseismic studies and have been analysed to determine their fundamental stellar parameters (Stello et al. 2013).

To increase the sample of giant stars with planets and to have more complete information of individual systems, we started a planet search programme among *Kepler* asteroseismic giant stars in 2010. Our advantage over other ground-based RV surveys of evolved stars is that we can determine reliable stellar properties, such as the stellar mass and radius, via asteroseismic analysis using the *Kepler* photometric data (Borucki et al. 2010). These characteristics are currently well known only for nine planet-hosting giant stars observed by space missions, which were found to have transiting planets (Huber et al. 2013; Lillo-Box et al. 2014; Ciceri et al. 2015; Ortiz et al. 2015; Quinn et al. 2015; Grunblatt et al. 2016, 2017, 2022; Jofré et al. 2020). Our sample of *Kepler* giant stars contains 95 targets, which is a statistically significant number given an expected giant-planet occurrence of $\sim 17\%$ (Ghezzi et al. 2018) for the mean stellar mass of our sample in the range $1.5\text{--}2 M_{\odot}$. We chose our targets from an initial list of giant stars from the *Kepler* Input Catalogue, which we ordered in brightness. Based on the *Kepler* photometry we removed binaries and targets that were clearly

not giant stars. Then we selected our sample from the brightest targets down to $V = 10.74$ mag and distributed it over four different telescopes in order to maximise the detection and to minimise the impact of telescope resources at a single site. The goal of our planet search programme is to characterise each individual target and conclude on the existence of sub-stellar companions. We published the discovery of a planetary candidate around the evolved low-mass *Kepler* giant star HD 175370 (Hrudková et al. 2017). Here, we report the discovery of two additional companions to *Kepler* giant stars from our planet search programme for which we were able to conclude on the nature of the companions. We found a brown dwarf candidate orbiting the red giant branch star KIC 3526061 and a stellar mass companion orbiting the red giant branch star HD 187878. KIC 3526061 is the most evolved system found to date having a sub-stellar companion with such a large eccentricity and wide separation.

This paper is organised as follows. In Sect. 2 we give an overview of our observations of KIC 3526061 and HD 187878, and describe the four different echelle spectrographs we used in this study. Section 3 is devoted to KIC 3526061, where we derive stellar parameters and the orbital solution, analyse stellar activity, and discuss our results, particularly the origin of a large orbital eccentricity. In a similar manner, we describe our analysis and results for HD 187878 in Sect. 4. In Sect. 5 we provide a brief summary and conclusions.

2. Observations and data reduction

We started observing KIC 3526061 in August 2012 using the Robert G. Tull Coudé cross-dispersed echelle spectrograph (TS2) of the 2.7m *Harlan J. Smith* Telescope at the McDonald Observatory in Texas, U.S. We obtained 17 spectra with a S/N of ~ 100 per pixel in the extracted spectrum. Since April 2018 we have also monitored this star using the fibre-fed High Efficiency and Resolution *Mercator* Echelle Spectrograph (HERMES) at the 1.2m *Mercator* Telescope on La Palma, Canary Islands, Spain. We obtained eight spectra with a S/N of ~ 80 per pixel in the extracted spectrum. The RV measurements from both sites are listed in Table 1.

We started observing HD 187878 in March 2010 using the coudé echelle spectrograph at the 2m *Alfred Jensch* Telescope at the Thüringer Landessternwarte Tautenburg (TLS), Germany. We obtained 54 spectra with a S/N of ~ 100 per pixel in the extracted spectrum. Since July 2011 we have monitored this star using the HERMES spectrograph. We obtained 25 spectra with a S/N of ~ 85 per pixel in the extracted spectrum. Since September 2020 we have observed this star with the Ondřejov Echelle Spectrograph (OES) installed at the 2m Perek telescope at the Astronomical Institute of the Czech Academy of Sciences in Ondřejov, Czech Republic. We obtained 21 spectra with a S/N of $\sim 30\text{--}180$ per pixel in the extracted spectrum. The RV measurements from all sites are listed in Table 2.

2.1. TLS data

The coudé echelle spectrograph at TLS provides a wavelength range of $4670\text{--}7400 \text{ \AA}$ and a spectral resolving power of 67 000. We reduced the data using standard IRAF² procedures (bias subtraction, flat-field correction, extraction of individual echelle

² The Image Reduction and Analysis Facility (IRAF) is distributed by the National Optical Astronomy Observatories, which are operated by the Association of Universities for Research in Astronomy, Inc., under cooperative agreement with the National Science Foundation.

¹ <http://exoplanet.eu/>

Table 1. Radial velocity measurements of KIC 3526061.

BJD (d)	RV (m s ⁻¹)	σ_{RV} (m s ⁻¹)
McDonald		
2456168.845738	-55.7	20.4
2456550.715116	-20.1	14.4
...		
HERMES		
2458218.683338	-27465.0	5.0
2458261.513262	-27419.0	3.0
...		

Notes. At the McDonald Observatory we used an iodine cell which resulted in RVs relative to a stellar template, while from the *Mercator* telescope the RVs are absolute. RVs were corrected for the barycentre motion, using the program BARCOR (<https://stelweb.asu.cas.cz/~marie/Barcor/>). The RV uncertainties correspond to instrumental errors. This table is available in its entirety at the CDS.

Table 2. Radial velocity measurements of HD 187878 from three different sites.

BJD (d)	RV (m s ⁻¹)	σ_{RV} (m s ⁻¹)
HERMES		
2455745.529925	-18026	2
2455771.640696	-18121	2
...		
TLS old		
2455279.578207	390.8	8.2
2455357.394732	443.7	9.1
...		
TLS new		
2456783.548644	470.0	17.1
2456797.355630	456.0	13.7
...		
Ondřejov		
2459108.399065	-496.5	24.5
2459124.276912	-494.2	28.9
...		

Notes. At TLS and Ondřejov we used an iodine cell which resulted in RVs relative to a stellar template, while with HERMES we obtained absolute RVs. RVs were corrected for the barycentre motion. The RV uncertainties correspond to instrumental errors. The difference between TLS new and old is explained in the text. This table is available in its entirety at the CDS.

orders, wavelength calibration, subtraction of scattered light, cosmic ray removal, and spectrum normalisation). We used an iodine absorption cell placed in the optical path just before the slit of the spectrograph as the wavelength reference. The calculation of the RVs largely followed the method outlined in Valenti et al. (1995), Butler et al. (1996), and Endl et al. (2000), and takes into account changes in the instrumental profile. We note that the measured RVs are relative to a stellar template which is an iodine-free spectrum and are not absolute values. In May 2014 a new echelle grating was mounted at the coude spectrograph at TLS. With the new set-up it was necessary to treat data as an independent data set, using a new stellar template as a reference. Throughout the paper we refer to data taken before

this change as ‘TLS old data’ and data taken after the change as ‘TLS new data’.

2.2. McDonald data

The TS2 coude echelle spectrograph at the McDonald Observatory provides a wavelength range of 3400–10 900 Å and a spectral resolving power of 60 000. We reduced the data using standard IRAF procedures and used an iodine absorption cell as the wavelength reference, as we did for the TLS data. More details about the TS2 spectrograph can be found in Tull et al. (1995).

2.3. HERMES data

For the HERMES spectrograph we used a simultaneous ThArNe wavelength reference mode in order to achieve RV measurements that were as accurate as possible. The wavelength range of HERMES is 3770–9000 Å. Before August 2018 we used the lower-resolution mode of HERMES, which provided us with a spectral resolving power of 62 000. In August 2018 the option of using a high-resolution fibre (HRF) mode with a simultaneous ThArNe wavelength reference became available. We thus started to observe in HRF mode, which provided a spectral resolving power of 85 000. More details about the HERMES spectrograph can be found in Raskin et al. (2011). We used a dedicated automated data reduction pipeline and RV toolkit (HERMESDRS) to reduce the data and calculate absolute RVs. The spectral mask of Arcturus on the velocity scale of the IAU RV standards was used for the cross-correlation.

2.4. Ondřejov data

The OES spectrograph in Ondřejov provides a wavelength range of 3750–9200 Å and a spectral resolving power of 50 000. More details about the OES spectrograph can be found in Koubský et al. (2004) and Kabáth et al. (2020). We reduced the data using standard IRAF procedures, and used an iodine absorption cell as the wavelength reference. RVs were calculated using the Velocity and Instrument Profile Estimator (VIPER)³ (Zechmeister et al. 2021), which is a PYTHON-based software for calculating the RVs of stellar spectra taken using iodine cell or other gas cells.

3. KIC 3526061

3.1. Stellar properties

KIC 3526061 has a visual magnitude of $m_V = 10.37 \pm 0.04$ mag (Høg et al. 2000). The parallax was determined from *Gaia* EDR3 data as 2.504 ± 0.012 mas (Gaia Collaboration 2016, 2021a), which implies an absolute magnitude $M_V = 2.36 \pm 0.04$ mag. Table 3 lists the stellar parameters known from the literature together with those determined in this work.

The basic stellar parameters were determined from a high-resolution ($R = 60\,000$) spectrum of KIC 3526061 taken without the iodine cell using the 2.7m telescope at the McDonald Observatory with a S/N of ~ 145 . For the spectrum analysis we used the Grid Search in Stellar Parameters (GSSP) code (Tkachenko 2015), which works in a very fast and efficient way. It employs the spectrum-synthesis method by comparing the observed spectrum with a library of synthetic spectra computed by SYNTLV (Tsymbal 1996) from atmosphere models on a grid of stellar

³ <https://github.com/mzechmeister/viper>

Table 3. Stellar parameters of KIC 3526061 from this work together with those known from the literature.

Parameter	Value	Reference	Parameter	Value	Reference
m_V (mag)	10.37 ± 0.04	Høg et al. (2000)	$\Delta\nu$ (μHz)	10.7 ± 0.3	Hekker et al. (2011) ^(a)
$B - V$ (mag)	0.96 ± 0.08	Høg et al. (2000)	$\Delta\nu$ (μHz)	10.73 ± 0.05	Mosser et al. (2014)
Parallax (mas)	2.5042 ± 0.0123	Gaia Collaboration (2021a)	$\Delta\nu$ (μHz)	10.64 ± 0.23	Pinsonneault et al. (2014)
M_V (mag)	2.36 ± 0.04	This work	$\Delta\nu$ (μHz)	10.670 ± 0.014	Huber et al. (2017) ^(b)
Distance (pc)	399 ± 2	This work	$\Delta\nu$ (μHz)	10.667 ± 0.004	Pinsonneault et al. (2018)
Distance (pc)	412^{+10}_{-18}	Rodrigues et al. (2014)	$\Delta\nu$ (μHz)	10.71	Vrard et al. (2018)
Distance (pc)	645 ± 88	Wang et al. (2016)	$\Delta\nu$ (μHz)	10.677 ± 0.016	Yu et al. (2018)
Distance (pc)	407^{+18}_{-18}	Huber et al. (2017) ^(b)	$\Delta\nu$ (μHz)	10.62 ± 0.05	Gaulme et al. (2020)
Distance (pc)	392.44 ± 12.70	Silva Aguirre et al. (2018)	ν_{max} (μHz)	129 ± 4	Hekker et al. (2011) ^(a)
T_{eff} (K)	4829^{+102}_{-102}	This work	ν_{max} (μHz)	127.52 ± 2.79	Pinsonneault et al. (2014)
T_{eff} (K)	4683 ± 77	Pinsonneault et al. (2014)	ν_{max} (μHz)	128.607 ± 0.639	Huber et al. (2017) ^(b)
T_{eff} (K)	4747 ± 5	Ness et al. (2016)	ν_{max} (μHz)	128.243 ± 0.012	Pinsonneault et al. (2018)
T_{eff} (K)	4747 ± 86	Huber et al. (2017) ^(b)	ν_{max} (μHz)	130.0	Vrard et al. (2018)
T_{eff} (K)	4770 ± 73	Pinsonneault et al. (2018)	ν_{max} (μHz)	128.74 ± 0.60	Yu et al. (2018)
T_{eff} (K)	4865 ± 100	Yu et al. (2018)	ν_{max} (μHz)	129.82 ± 0.25	Gaulme et al. (2020)
[Fe/H] (dex)	$0.12^{+0.10}_{-0.11}$	This work	Age (Gyr)	8.66 ± 1.06	Ness et al. (2016)
[Fe/H] (dex)	0.23 ± 0.05	Pinsonneault et al. (2014)	Age (Gyr)	5.309 ± 0.001	Pinsonneault et al. (2018)
[Fe/H] (dex)	0.13 ± 0.11	Hawkins et al. (2016)	Age (Gyr)	5.169 ± 1.270	Silva Aguirre et al. (2018)
[Fe/H] (dex)	0.237 ± 0.004	Ness et al. (2016)	M_* (M_{\odot})	1.48 ± 0.20	Mosser et al. (2014)
[Fe/H] (dex)	0.157 ± 0.060	Huber et al. (2017) ^(b)	M_* (M_{\odot})	$1.26^{+0.13}_{-0.11}$	Pinsonneault et al. (2014)
[Fe/H] (dex)	0.224 ± 0.027	Pinsonneault et al. (2018)	M_* (M_{\odot})	1.11 ± 1.02	Ness et al. (2016)
[Fe/H] (dex)	0.23 ± 0.15	Yu et al. (2018)	M_* (M_{\odot})	1.274 ± 0.046	Pinsonneault et al. (2018)
ν_{turb} (km s^{-1})	$1.13^{+0.27}_{-0.21}$	This work	M_* (M_{\odot})	1.291 ± 0.061	Silva Aguirre et al. (2018)
ν_{turb} (km s^{-1})	1.037 ± 0.081	Hawkins et al. (2016)	M_* (M_{\odot})	1.42 ± 0.041	Vrard et al. (2018)
ν_{macro} (km s^{-1})	$4.82^{+0.91}_{-4.82}$	This work	M_* (M_{\odot})	1.38 ± 0.07	Yu et al. (2018)
$\nu \sin i$ (km s^{-1})	$1.32^{+4.20}_{-0.33}$	This work	M_* (M_{\odot})	1.42 ± 0.09	Gaulme et al. (2020)
$\log g$ (dex)	$3.09^{+0.32}_{-0.33}$	This work	M_* (M_{\odot})	$1.220^{+0.566}_{-0.565}$	Sayeed et al. (2021)
$\log g$ (dex)	3.001 ± 0.011	Pinsonneault et al. (2014)	R_* (R_{\odot})	$5.86^{+0.24}_{-0.22}$	Pinsonneault et al. (2014)
$\log g$ (dex)	2.94 ± 0.01	Ness et al. (2016)	R_* (R_{\odot})	$5.854^{+0.104}_{-0.104}$	Huber et al. (2017) ^(b)
$\log g$ (dex)	3.015 ± 0.004	Huber et al. (2017) ^(b)	R_* (R_{\odot})	5.797 ± 0.016	Pinsonneault et al. (2018)
$\log g$ (dex)	3.017 ± 0.006	Pinsonneault et al. (2018)	R_* (R_{\odot})	5.834 ± 0.121	Silva Aguirre et al. (2018)
$\log g$ (dex)	3.016 ± 0.005	Silva Aguirre et al. (2018)	R_* (R_{\odot})	6.02 ± 0.11	Yu et al. (2018)
$\log g$ (dex)	3.021 ± 0.007	Yu et al. (2018)	R_* (R_{\odot})	6.09 ± 0.12	Gaulme et al. (2020)
$\log g$ (dex)	3.02 ± 0.01	Gaulme et al. (2020)	R_* (R_{\odot})	$5.673^{+0.152}_{-0.146}$	Sayeed et al. (2021)
$\log g$ (dex)	3.012 ± 0.200	Sayeed et al. (2021)	Status	RGB ^(c)	Mosser et al. (2014)
L (L_{\odot})	16.4 ± 1.4	This work	Status	RGB ^(c)	Ness et al. (2016)
L (L_{\odot})	15.716 ± 1.325	Silva Aguirre et al. (2018)	Status	RGB ^(c)	Elsworth et al. (2017)
			Status	non He-core burning	Huber et al. (2017) ^(b)
			Status	RGB ^(c)	Vrard et al. (2018)
			Status	RGB ^(c)	Yu et al. (2018)

Notes. ^(a)OCT I method with uncertainties based on synthetic results; ^(b) $\Delta\nu$ corrected direct method; ^(c)RGB = red giant branch star.

parameters. SYNTHV is a spectrum-synthesis code based on plane-parallel atmospheres and working in a non-local thermodynamic equilibrium regime. It has the advantage that for each chemical element different abundances can be considered.

The free stellar parameters in our analysis were the stellar effective temperature, T_{eff} ; the stellar gravity, $\log g$; the metallicity, [Fe/H]; the microturbulent velocity, ν_{turb} ; the macroturbulent velocity, ν_{macro} ; and the projected rotational velocity, $\nu \sin i$. The goodness of the fit as well as the parameter uncertainties were calculated from χ^2 -statistics (Lehmann et al. 2011).

The GSSP code cannot adjust the observed continuum, except for a constant factor, which has a limitation in analysing cool stars or the blue part of spectra that includes the higher Balmer lines. Therefore, we used it only in grid mode and used our own MIDAS programs for fitting (Lehmann et al. 2011). We restricted the wavelength range to 4369–5785 Å, which provided best results concerning continuum value, S/N, and overlap of the orders.

We encountered a large dependency between the projected rotational velocity and the macroturbulent velocity. This was not surprising because for slow rotators there is a trade off between the two parameters. Therefore, we left both param-

eters free in the following analysis. We determined T_{eff} , $\log g$, ν_{turb} , [Fe/H], $\nu \sin i$, and ν_{macro} and then optimised the abundances of individual elements. Both steps were repeated in an iterative way. The resulting parameters are shown in Table 3, where we also list the results of previous studies. The resulting $\nu_{\text{macro}} = 4.82^{+0.91}_{-4.82} \text{ km s}^{-1}$ agrees very well with the typical value for red giant stars of $\sim 5 \text{ km s}^{-1}$ (Gray 1988).

The results of the abundances of chemical elements are listed in Table 4. All abundances determined in this work agree within the error bars with the values from Hawkins et al. (2016), see also Fig. 1.

3.2. Brown dwarf candidate KIC 3526061 b

We monitored KIC 3526061 for nearly nine years and acquired 17 RV measurements at the McDonald Observatory and eight RV measurements at the *Mercator* telescope (see Table 1 and Fig. 2). Our RV measurements show changes that could be caused by a sub-stellar companion. In order to access the nature of the companion we used the code PYANETI (Barragán et al. 2019), which employs a Bayesian approach combined with Markov chain Monte Carlo sampling to estimate the companion

Table 4. Abundances of KIC 3526061 relative to solar composition determined in this work together with those known from the literature.

Reference	Na	Mg	Si	Ca	Sc	Ti	V
1	+0.44 ^{+0.72} _{-0.97}	+0.13 ^{+0.19} _{-0.25}	+0.28 ^{+0.25} _{-0.42}	+0.18 ^{+0.42} _{-0.58}	+0.43 ^{+0.43} _{-0.53}	+0.25 ^{+0.17} _{-0.18}	+0.28 ^{+0.26} _{-0.29}
2	+0.12 ± 0.09	+0.21 ± 0.12	+0.18 ± 0.07	+0.07 ± 0.07		+0.17 ± 0.09	+0.15 ± 0.05
	Cr	Mn	Fe	Co	Ni	Ce	Nd
1	+0.16 ^{+0.18} _{-0.20}	+0.35 ^{+0.36} _{-0.44}	+0.14 ^{+0.10} _{-0.10}	+0.25 ^{+0.28} _{-0.32}	+0.26 ^{+0.25} _{-0.27}	+0.24 ^{+0.46} _{-0.94}	+0.26 ^{+0.40} _{-0.62}
2	+0.16 ± 0.12	+0.14 ± 0.00	+0.13 ± 0.11	+0.15 ± 0.05	+0.22 ± 0.02		

References. (1) This work; (2) [Hawkins et al. \(2016\)](#).

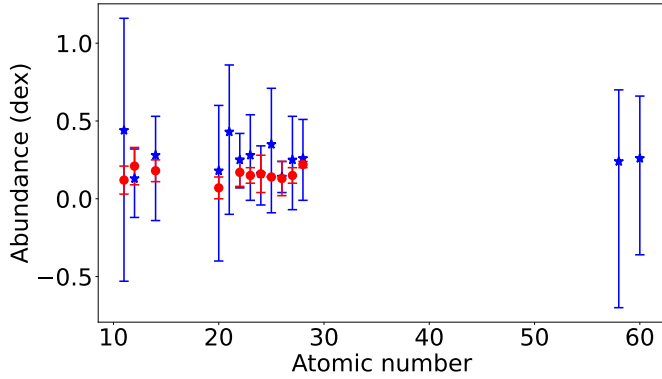


Fig. 1. Abundances of KIC 3526061 relative to solar composition determined in this work (blue stars) and in [Hawkins et al. \(2016\)](#) (red filled circles).

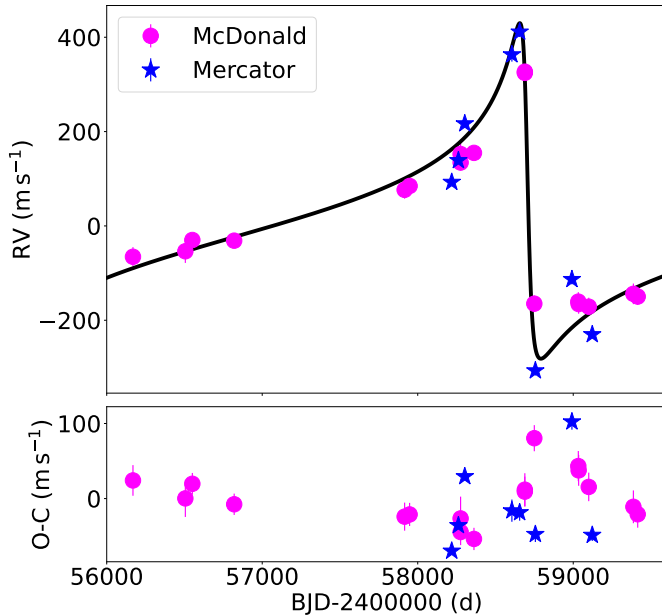


Fig. 2. Radial velocity measurements of KIC 3526061. *Top*: data obtained from August 2012 to July 2021 using the TS2 spectrograph at the McDonald Observatory, Texas, and the HERMES spectrograph at Mercator, La Palma. The solid curve represents the Keplerian orbital solution. *Bottom*: RV residuals and error bars after removing the brown dwarf orbital solution.

parameters. We derived the best-fitting orbital solution for KIC 3526061 b including the data from both data sets. A parameter space with 500 Markov chains was explored to generate a posterior distribution of 20 000 independent points for each

Table 5. Orbital parameters of KIC 3526061 b.

Parameter	Value	Unit
Fitted		
Period	3552 ⁺¹⁵⁸ ₋₁₃₅	d
T_0	2 458 708.1 ^{+2.0} _{-1.9}	d
K	355.7 ^{+5.1} _{-5.0}	m s^{-1}
e	0.85 ^{+0.01} _{-0.01}	
ω	75.7 ^{+1.3} _{-1.3}	deg
Derived		
$M \sin i$	18.15 ^{+0.44} _{-0.44}	M_{Jup}
$T_{\text{periastron}}$	2 458 701.7 ^{+2.4} _{-2.2}	d
a	5.14 ± 0.16	AU
Other parameters		
RV_0^{McD}	9.7 ^{+5.8} _{-5.9}	m s^{-1}
RV_0^{HERMES}	-27 557.9 ^{+3.2} _{-3.3}	m s^{-1}
rms _{Total}	40.6	m s^{-1}
rms _{McD}	32.9	m s^{-1}
rms _{HERMES}	53.3	m s^{-1}

model parameter. We set uniform priors for all fitted parameters. We accounted for the RV zero points, RV_0 , between the two different instruments and included jitter terms. We fitted for the orbital period, P ; time of minimum conjunction, T_0 ; eccentricity, e ; periastron longitude, ω ; and semi-amplitude of the RV curve, K . The inferred parameters are given in Table 5. They are defined as the mean and 68 % region of the credible interval of the posterior distributions for each fitted parameter. In Table 5, the scatter of RV residuals around the orbital solution, the rms, is given for all data and for data from each instrument. We also used FOTEL ([Hadrava 2004](#)) to independently check the orbital solution, and found that the resulting parameters were the same as for PYANETI within the uncertainties. In Fig. 2 we show the RV measurements with the orbital solution (top panel) and RV residuals with error bars (bottom panel). Phase-folded RV variations for the orbital solution and the orbital fit are displayed in Fig. 3.

We searched for additional periods in residual RV data using the program PERIOD04 ([Lenz & Breger 2005](#)) based on the Fourier analysis, where multiple periods can be found via a pre-whitening procedure. A periodogram search out to the Nyquist frequency in residual RV data showed no additional significant frequencies (see Fig. 4). The highest amplitude in the Fourier spectrum corresponds to a false alarm probability of greater than 50% using the criterion of [Kuschnig et al. \(1997\)](#).

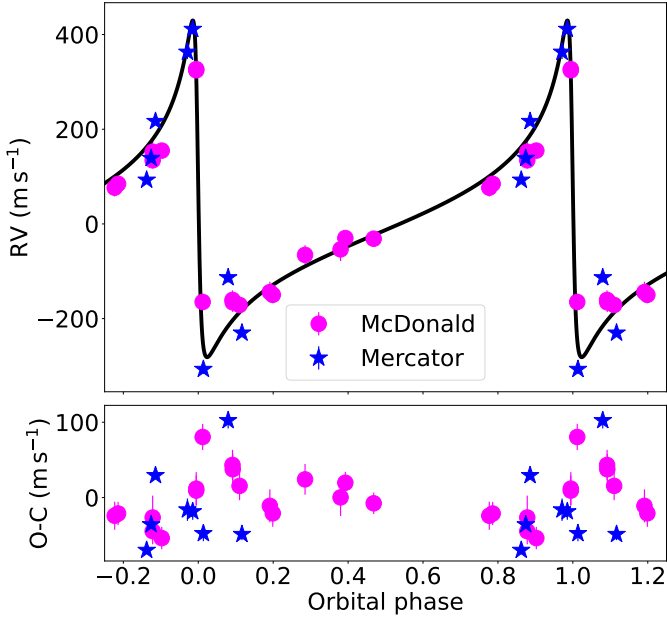


Fig. 3. Phased RV measurements of KIC 3526061. *Top*: data plotted with corresponding error bars and phased to the orbital period of 3552 d. The Keplerian orbital solution is overplotted with a solid curve. *Bottom*: RV residuals and error bars after removing the brown dwarf orbital solution.

3.2.1. Amplitude of stellar oscillations

The scatter of RV residuals after fitting the companion’s orbit is 40.6 m s^{-1} , which is higher than instrumental errors of our RV measurements. This scatter cannot be solely due to solar-like oscillations. According to the scaling relations of [Kjeldsen & Bedding \(1995\)](#), the velocity amplitude for stellar oscillations is expected to be $v_{\text{osc}} = ((L_*/L_\odot)/(M_*/M_\odot))^{23.4} \text{ cm s}^{-1}$. We derived the stellar luminosity $L_* = 16.4 \pm 1.4 L_\odot$ using our estimated stellar effective temperature of $T_{\text{eff}} = 4829 \text{ K}$ and the stellar radius of [Pinsonneault et al. \(2018\)](#). We used this luminosity and the stellar mass of [Vrard et al. \(2018\)](#) to calculate a velocity amplitude of $v_{\text{osc}} = 2.7 \text{ m s}^{-1}$. We chose the stellar mass of [Vrard et al. \(2018\)](#) and the stellar radius of [Pinsonneault et al. \(2018\)](#) for their smallest uncertainties of all values presented in Table 3. We also used Eqs. (7) and (8) from [Kjeldsen & Bedding \(1995\)](#) to predict a velocity amplitude based on the luminosity amplitude from the *Kepler* light curves, and derived $v_{\text{osc}} = 1.9 \text{ m s}^{-1}$. Both velocity amplitude estimates are much smaller than the scatter of the RV residuals. The scatter of RV residuals is 32.9 m s^{-1} for the McDonald data and 53.3 m s^{-1} for the Mercator data. As the McDonald data have lower scatter, we used them to derive an orbital solution independent of the Mercator data. We followed a similar procedure to the one described above. The resulting best-fitting orbital period was $P = 4581 \pm 400 \text{ d}$ and eccentricity $e = 0.91 \pm 0.04$, and surprisingly the scatter of RV residuals was only 9 m s^{-1} . This value is closer to our velocity amplitude estimates and is even lower than the instrumental errors of RV measurements. This indicates good long-term stability of RVs from the TS2 spectrograph at the McDonald Observatory over the time period of nine years.

However, the period based only on the McDonald data is quite different than the period obtained based on the combined data. This shows that in fact the uncertainty of the period is much larger than the value given in Table 5. The large error of the

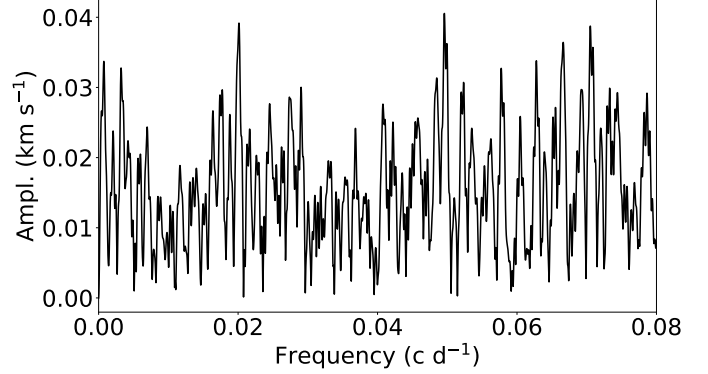


Fig. 4. Frequency amplitude spectrum of residual RV data of KIC 3526061 after removing the Keplerian orbital solution.

orbital period arises from a combination of having a time base of observations close to the orbital period and sparse sampling of observations around the periastron passage. It is obvious that to refine the orbital solution more RV measurements from stable spectrographs such as TS2 at the McDonald Observatory would be needed, and particularly observations around the time of the predicted periastron passage.

3.2.2. Mass of companion

Using a stellar mass of $1.42 \pm 0.041 M_\odot$ ([Vrard et al. 2018](#)) the derived minimum mass of the companion is $M \sin i = 18.15 \pm 0.44 M_{\text{Jupiter}}$. [Jorissen et al. \(2020\)](#) classified KIC 3526061 as a spectroscopic binary based on unpublished RVs. We used their data to make a common orbital solution with our data, which resulted in a scatter of RV residuals after fitting the companion’s orbit of 53.4 m s^{-1} . This is a larger scatter than without including the data of [Jorissen et al. \(2020\)](#). In addition, their RVs have uncertainties of $\sim 45 \text{ m s}^{-1}$, which is larger than for our data. For these two reasons we did not include their data in our analysis. However, we confirm that their data are consistent with our results, giving the derived minimum mass of the companion in the common orbital solution of $18.27 \pm 0.44 M_{\text{Jupiter}}$.

The unknown orbital inclination leaves an open question as to the real nature of the companion. Under the assumption that inclination angles are randomly distributed on the sky, there is only a 2.6% chance for the companion’s mass to be greater than $80 M_{\text{Jupiter}}$, which has been proposed as the dividing line between sub-stellar and stellar objects ([Burrows et al. 2001](#); [Hatzes & Rauer 2015](#); [Chen & Kipping 2017](#)). This means that KIC 3526061 b is very likely a sub-stellar object, either a brown dwarf or a giant planet. The masses of brown dwarfs are defined as being in the range $13\text{--}80 M_{\text{Jupiter}}$ ([Burrows et al. 2001](#)), where objects sustain deuterium burning through nuclear fusion for typically 0.1 million years, but are below the ignition limit of hydrogen at $75\text{--}80 M_{\text{Jupiter}}$. Another division between giant planets and brown dwarfs is based on formation, where the mass domains overlap since the minimum brown dwarf mass is a few Jupiter masses and the maximum exoplanet mass can be as high as $\sim 30 M_{\text{Jupiter}}$ ([Chabrier et al. 2014](#)). [Whitworth \(2018\)](#) argued that, as regards their formation, brown dwarfs should not be distinguished from hydrogen-burning stars. On the other hand, [Hatzes & Rauer \(2015\)](#) suggested that, based on the mass-density relationship of sub-stellar objects, all objects in the mass range $0.3\text{--}60 M_{\text{Jupiter}}$ should be considered giant planets. This was further corroborated by [Chen & Kipping \(2017\)](#) who found

that brown dwarfs follow the same trend as giant planets in the mass-radius diagram.

3.2.3. Transit probability, depth, and duration

In order to calculate the probability, depth and duration of a potential transit, we first estimated the sub-stellar companion's radius. We used the mass-radius relationship for the Jovian regime in the form $R_p \propto M_p^{-0.04}$ given by [Chen & Kipping \(2017\)](#), which resulted in the companion radius of $0.89 R_{\text{Jupiter}}$. Assuming an inclination of $i = 90^\circ$ and ignoring limb darkening effects, we calculated a transit probability of 3.5% using Eq. (5) in [Kane & von Braun \(2008\)](#), a transit depth of 0.0244% or 244 ppm, and a transit duration of 0.9 d. KIC 3526061 as an evolved star presents a photometric variability of about 700 ppm in the *Kepler* light curve; that is larger than the expected transit depth, which complicates searching for a potential transit signal. The real difficulty, however, comes from the closeness of the transit duration and a timescale of intrinsic variations making them difficult to disentangle. Moreover, currently we do not have enough knowledge about potential transit times, due to the large uncertainty on the orbital period.

3.2.4. Wide orbit

KIC 3526061 b has one of the longest known orbital period of sub-stellar companions that orbit a giant star. We show the position of KIC 3526061 b in the semi-major axis versus minimum planet mass diagram in Fig. 5. KIC 3526061 b is placed in a barely populated region of the diagram. More distant or similarly distant companions were discovered by [Quirrenbach et al. \(2011\)](#) around ν Oph with a companion minimum mass of $24.5 M_{\text{Jupiter}}$ at the orbital distance of $a = 5.89$ AU, by [Wang et al. \(2014\)](#) around HD 14067 with a companion minimum mass of $9 M_{\text{Jupiter}}$ at the orbital distance of $a = 5.3$ AU, by [Jones et al. \(2017\)](#) around HIP 67537 with a companion minimum mass of $11.1 M_{\text{Jupiter}}$ at the orbital distance of $a = 4.91$ AU, and by [Adamów et al. \(2018\)](#) around HD 238914 with a companion minimum mass of $6 M_{\text{Jupiter}}$ at the orbital distance of $a = 5.7$ AU.

3.2.5. Origin of a large orbital eccentricity

KIC 3526061 is the most evolved system found having a sub-stellar companion with such a large eccentricity and wide separation (see Fig. 6). The orbital eccentricity 0.85 ± 0.01 of KIC 3526061 b is the second largest for a sub-stellar companion orbiting a giant star. So far only one planetary companion, HD 76920 b with $M \sin i = 3.13^{+0.41}_{-0.43} M_{\text{Jupiter}}$ and semimajor axis 1.091 AU, orbiting a red giant star was found to have a higher eccentricity of 0.8782 ± 0.0025 ([Wittenmyer et al. 2017](#); [Bergmann et al. 2021](#)).

The origin of such a highly eccentric orbit is linked with the formation and dynamical history of KIC 3526061 b. Two main mechanisms for the formation of wide-orbit giant companions within protoplanetary disks have been proposed: top-down formation by gravitational disk instability (e.g., [Boss 1997](#)) and bottom-up formation by core accretion (e.g., [Pollack et al. 1996](#)). Planets are expected to form on circular coplanar orbits within protoplanetary disks via a core accretion, but can develop non-zero eccentricities through a planet-planet scattering (e.g., [Chatterjee et al. 2008](#); [Ford & Rasio 2008](#)), secular Kozai-Lidov perturbations with a massive outer companion (e.g., [Naoz 2016](#)),

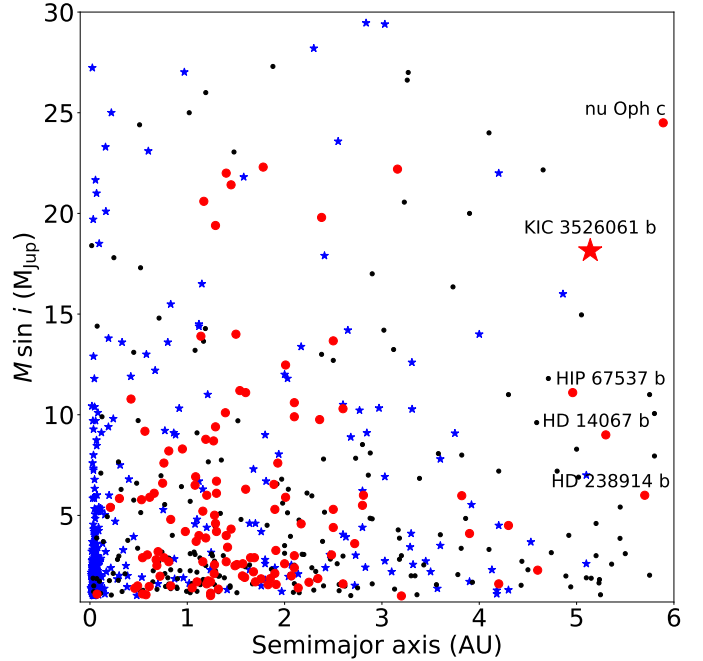


Fig. 5. Minimum planet mass vs. semi-major axis for known giant planets ($M \sin i \geq 1.0 M_{\text{Jupiter}}$) with a semi-major axis smaller than 6 AU. The black dots and the blue stars correspond to main sequence host stars (<http://exoplanet.eu/>) and the red filled circles correspond to giant host stars (<https://www.lsw.uni-heidelberg.de/users/sreffert/giantplanets/giantplanets.php>). The blue stars are transiting systems for which the true mass of the companion is shown. The red star shows the position of KIC 3526061 b.

or planet-disk interactions (e.g., [Goldreich & Sari 2003](#)). However, there are no indications of additional massive companions in the RV data of KIC 3526061. We also used the SIMBAD astronomical database ([Wenger et al. 2000](#)) and checked all sources within 5 arcmin of KIC 3526061, and found no targets with compatible parallax and proper motion. The scenario of a captured free-floating sub-stellar companion is also unlikely. According to simulations by [Parker et al. \(2017\)](#), free-floating planets are usually captured in much wider orbits. In a planet-planet scattering scenario, a second sub-stellar companion of a comparable mass would have been ejected from the system as the result of a close encounter with KIC 3526061 b, pushed outwards into a long-period orbit that is beyond our current detection limit, or engulfed by the star. The parameter space of a putative second companion is limited by the highly eccentric orbit of KIC 3526061 b, which is in the range 0.77–9.51 AU, or 28–349 R_* .

KIC 3526061 b is a sub-stellar companion on a wide orbit, where occurrence rates are low and there are orders of magnitude fewer discoveries compared to short-period systems; therefore, population-level studies might give us a better understanding of the formation of KIC 3526061 b. [Bowler et al. \(2020\)](#) combined new high-contrast imaging observations with astrometry to test for differences in the population-level eccentricity distributions of 27 long-period giant planets and brown dwarfs between 5 and 100 AU. Their analysis revealed that low-mass companions ($< 15 M_{\text{Jupiter}}$) and low mass ratio systems ($M_2/M_1 < 0.01$) preferentially have lower eccentricities, similar to the population of warm Jupiters at small separations, and the brown dwarf companions ($15\text{--}75 M_{\text{Jupiter}}$) and higher mass ratio systems ($M_2/M_1 = 0.01\text{--}0.2$) exhibit higher eccentricities. Their

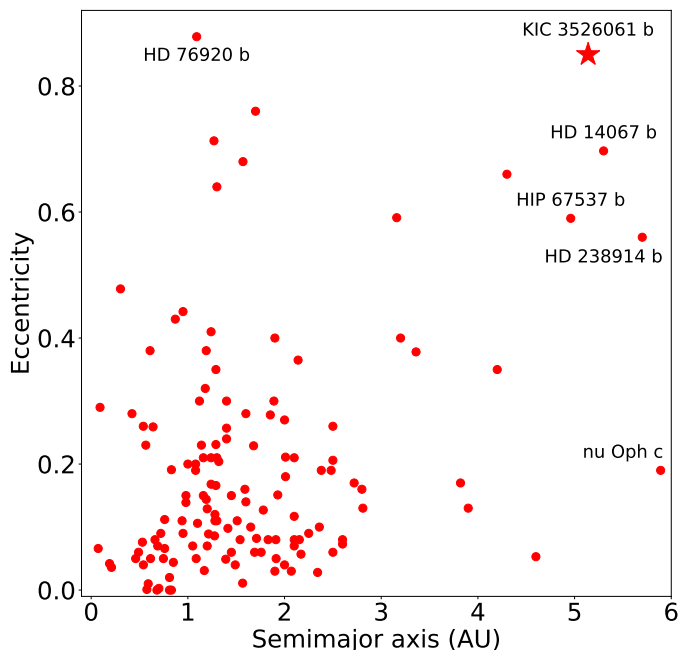


Fig. 6. Eccentricity vs. semi-major axis for all sub-stellar companions known around giant host stars (source: <https://www.lsw.uni-heidelberg.de/users/sreffert/giantplanets/giantplanets.php>). The red star shows the position of KIC 3526061 b.

explanation is that these populations predominantly form in distinct manners: the planetary-mass companions originate in disks and form via a core accretion, while brown dwarf companions represent the low-mass ratio end of binary star formation.

The mass ratio of the KIC 3526061 system is 0.0122, which places it in higher mass ratio systems according to [Bowler et al. \(2020\)](#) and points to the formation of KIC 3526061 b via a gravitational instability similar to that for the star formation. This is also supported by other studies. [Nielsen et al. \(2019\)](#) presented statistical results from the first 300 stars in the GPIES survey. They found that giant planets follow a bottom-heavy mass distribution and favour smaller semimajor axes, while brown dwarfs exhibit just the opposite behaviour, which points to the formation of giant planets by core or pebble accretion, and formation of brown dwarfs by gravitational instability. [Wagner et al. \(2019\)](#) analysed the underlying relative mass distribution of sub-stellar companions using survival analysis and concluded that core accretion is the primary mechanism for forming companions less massive than $\sim 10\text{--}20 M_{\text{Jupiter}}$, and that gravitational instability is the primary mechanism for forming higher-mass companions. [Ma & Ge \(2014\)](#) found that brown dwarfs with masses lower than $\sim 43 M_{\text{Jupiter}}$ have an eccentricity distribution consistent with giant planets in the mass–eccentricity diagram, while brown dwarfs with masses above $\sim 43 M_{\text{Jupiter}}$ have the star-like eccentricity distribution. They concluded that these results support the idea that brown dwarfs below this mass limit form in protoplanetary discs around host stars; above this mass limit they form like stellar binary systems. They also noted that their sample is not sufficient to exclude the possibility that a small number of brown dwarfs in each of the two mass regions may form in an opposite formation mechanism.

Based on the population-level studies it seems more likely that KIC 3526061 b was formed via a gravitational instability, which is also consistent with the findings of [Ma & Ge \(2014\)](#),

because we only have a minimum mass estimate for KIC 3526061 b. However, it is not excluded that KIC 3526061 b formed via a core accretion and developed such a large eccentricity via planet-planet scattering, for example. In addition, most direct imaging surveys have preferentially focused on young stars, and it is not clear whether the population-level eccentricities of sub-stellar companions evolve over time or are established at young ages ([Bowler et al. 2020](#)). KIC 3526061, as the most evolved system found having a sub-stellar companion with such a large eccentricity and wide separation (see Fig. 6), might provide a probe of the dynamical evolution of such systems over time.

3.3. Stellar activity analysis of KIC 3526061

3.3.1. Photometric variations

We analysed the *Kepler* photometry of KIC 3526061 in order to check whether there are any stellar activity features such as rotational modulation seen in the light curve. The star was observed by the *Kepler* satellite ([Borucki et al. 2010](#)) starting in May 2009 and for all quarters during the main *Kepler* mission. We used presearch data conditioning simple aperture photometry (PDCSAP) light curves ([Smith et al. 2012](#); [Stumpe et al. 2012](#)) downloaded from the Mikulski Archive for Space Telescopes ([Thompson et al. 2016](#)). In order to remove systematic trends in light curves, multi-scale cotrending basis vectors were used. They were built from the most common systematic trends observed in each quarter of the *Kepler* data. For light curve retrieval we made use of the following packages: LIGHTKURVE ([Lightkurve Collaboration 2018](#)), ASTROPY ([The Astropy Collaboration 2018](#)), and ASTROQUERY ([Ginsburg et al. 2019](#)). The orbital period of KIC 3526061 b is approximately twice as long as the time span of the *Kepler* data. We have not detected any trends that suggest there are photometric variations with the orbital period.

KIC 3526061 has also been observed in sectors 14 and 26 of the Transiting Exoplanet Survey Satellite (TESS; [Ricker et al. 2014](#)). We used PDCSAP light curves as above for the *Kepler* data, and found neither long-term variations nor evidence of transit events.

3.3.2. Spectral line bisector analysis

Inhomogeneous features on the stellar surface can create variable asymmetries in spectral line profiles as a star rotates. This asymmetry can be described with the line bisector, which consists of midpoints of horizontal line segments extending across a line profile. Typically, due to stellar granulation, the red wing of a stellar line is depressed, which causes a bisector to have a positive slope and curve to the right near the continuum level.

For the McDonald data, we used the fxcor task in IRAF to derive a cross-correlation function (CCF) for each spectrum. We used a spectral range 4440–4660, 6100–6260, and 6340–6427 Å, where no iodine and telluric lines were present, and where we obtained the most accurate results. Then we calculated a bisector for each individual CCF.

For the Mercator data we used a CCF of the HERMESDRS data reduction pipeline to calculate bisectors. The CCF was typically based on ~ 1655 spectral lines for each spectrum which results in very good accuracy for the bisector measurement. As we are interested in relative and not absolute bisector measurements, using an average of many lines is appropriate for studying variations of line bisectors with time

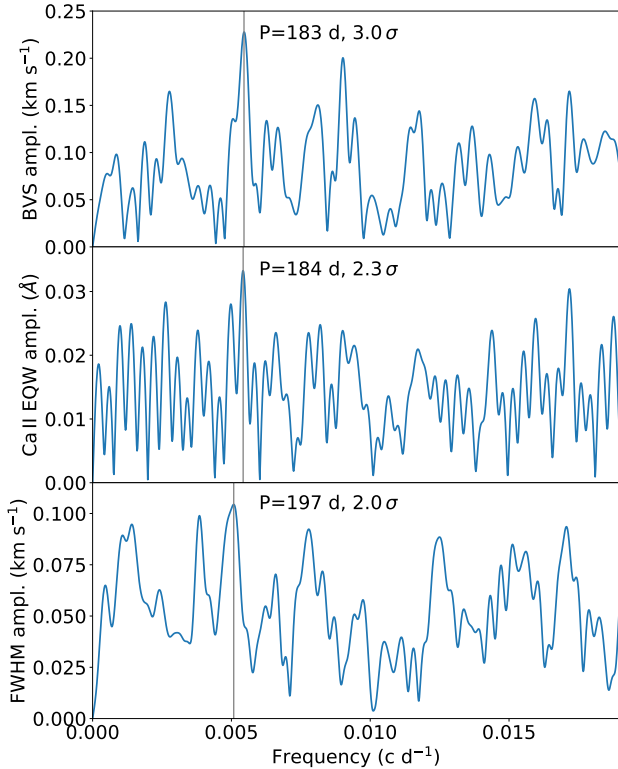


Fig. 7. Frequency amplitude spectra for KIC 3526061. *Top*: bisector velocity spans. *Middle*: equivalent width of the Ca II triplet lines. *Bottom*: full width at half maximum of spectral line shapes. For all three quantities we found variations on a similar timescale.

(e.g., [Martínez Fiorenzano et al. 2005](#); [Nowak et al. 2013](#)). We used normalised bisectors for both data sets for the subsequent analysis.

Bisector changes can be detected from bisector velocity span (BVS) measurements, which consist in measuring the difference between bisectors at two different flux levels of a spectral line ([Hatzes et al. 2015](#)). We measured the BVS of the spectral profile using the difference of the average bisector values between flux levels of 0.16–0.36 and 0.68–0.88 of the continuum value, which means that we avoided the spectral core and wing, where errors of the bisector measurements are larger.

We searched for periods in the BVS variations using the program PERIOD04 ([Lenz & Breger 2005](#)). The frequency spectrum is displayed in the top panel of Fig. 7. The most significant peak was found at the frequency $0.005453 \text{ c d}^{-1}$, corresponding to a period of $P = 183 \text{ d}$, with a 3.0σ significance and a false alarm probability of 0.016.

3.3.3. Spectral line shape analysis

In addition to the spectral line bisector analysis, there are other quantities that can be measured to evaluate the stellar activity over the rotation period of the star. We measured a full width at half maximum (FWHM) of each CCF derived as described in the previous section to access if there are any changes of spectral line shapes.

We searched for periods in the FWHM variations using the program PERIOD04 ([Lenz & Breger 2005](#)). The frequency spectrum is displayed in the bottom panel of Fig. 7. The most significant peak was found at the frequency 0.00508 c d^{-1} , corresponding to a period of $P = 197 \text{ d}$, with a 2.0σ significance.

3.3.4. Chromospheric activity

The equivalent width (EQW) variations of the Ca II H & K lines are often used as a chromospheric activity indicator. They are sensitive to stellar activity, which in turn may affect the measured RV variations. In chromospherically active stars the Ca II H & K lines show a typical line core reversal ([Pasquini et al. 1988](#)). Spectra of KIC 3526061 from both sites have a low S/N in a region of the Ca II H & K lines, which complicates the analysis of possible emission features in line cores. Instead, the Ca II triplet lines are often used to measure chromospheric activity ([Hatzes et al. 2003](#); [Lee et al. 2013](#)).

[Linsky et al. \(1979\)](#) showed that the Ca II 8542 Å line was suitable as a diagnostic of stellar chromospheric activity. The Ca II 8662 Å line is also suitable for this purpose and, unlike Ca II 8498 Å and Ca II 8542 Å, is uncontaminated by atmospheric water vapour lines near the line core ([Larson et al. 1993](#)).

For the McDonald data, we measured the EQW at the central part of the Ca II 8542 Å line from 8540.97 to 8543.24 Å and of the Ca II 8662 Å line from 8661.0 to 8663.27 Å. We averaged the two measurements, and searched for periods using the program PERIOD04 ([Lenz & Breger 2005](#)). The frequency spectrum is displayed in the middle panel of Fig. 7. The most significant peak was found at the frequency $0.005422 \text{ c d}^{-1}$, corresponding to a period of $P = 184 \text{ d}$, with a 2.3σ significance.

In the Mercator data we measured the EQW at the central part of the Ca II 8498 Å line from 8497.52 to 8498.58 Å; of the Ca II 8542 Å line from 8541.63 to 8542.60 Å; and of the Ca II 8662 Å line in two different ranges, 8661.55–8662.73 Å and 8661.0–8663.27 Å. We did not find any significant peaks in frequency spectra. This could be also due to a small number of measurements; only eight spectra were taken of KIC 3526061 at the *Mercator* telescope.

3.3.5. Rotation period of KIC 3526061

In Fig. 7 we show frequency amplitude spectra of our measurements of bisector velocity spans, a FWHM of spectral line shapes, and equivalent widths of the Ca II triplet lines (for details see previous sections). We found variations on a similar timescale of about 183 days in all three quantities. If these variations were related to a stellar rotation period, and we assumed a stellar rotation period of 183 days and the stellar radius of [Pinsonneault et al. \(2018\)](#), then the projected rotational velocity would be $v \sin i = 1.6 \text{ km s}^{-1}$. This would lift the degeneracy described in Sect. 3.1 between the projected rotational velocity and the macroturbulent velocity. However, we should be cautious because the signal is weak, is based only on 25 observations spread over nine years, and in addition has a period of about half a year. The variations can be due to changes in the instrumental profile, which varies between individual observing runs and is the most likely cause of variations in all three measured quantities. This is especially true of the McDonald data since there are moving components in the Tull spectrograph, such as the echelle grating and prisms, which are changed for different setups according to the observer’s needs. At this moment we cannot draw any conclusions regarding the real reason of the variations.

4. HD 187878

4.1. Stellar properties

HD 187878 has a visual magnitude of $m_V = 7.13 \pm 0.01 \text{ mag}$ ([Høg et al. 2000](#)). The parallax was determined from

Table 6. Stellar parameters of HD 187878 from this work together with those known from the literature.

Parameter	Value	Reference
m_V (mag)	7.13 ± 0.01	Høg et al. (2000)
$B - V$ (mag)	0.98 ± 0.02	Høg et al. (2000)
Parallax (mas)	5.1501 ± 0.0597	Gaia Collaboration (2021a)
M_V (mag)	0.69 ± 0.03	This work
Distance (pc)	194 ± 2	This work
Distance (pc)	201.75887	Cruzalèbes et al. (2019)
T_{eff} (K)	5168^{+65}_{-63}	This work
T_{eff} (K)	5053	McDonald et al. (2012)
T_{eff} (K)	5091 ± 80	Thygesen et al. (2012)
T_{eff} (K)	5003.38	Cruzalèbes et al. (2019)
[Fe/H] (dex)	$0.00^{+0.06}_{-0.07}$	This work
[Fe/H] (dex)	0.00 ± 0.15	Thygesen et al. (2012)
v_{turb} (km s ⁻¹)	$1.56^{+0.12}_{-0.16}$	This work
v_{turb} (km s ⁻¹)	1.37 ± 0.15	Thygesen et al. (2012)
v_{macro} (km s ⁻¹)	0.6 ± 1	Thygesen et al. (2012)
$v \sin i$ (km s ⁻¹)	$4.79^{+0.46}_{-0.46}$	This work
$v \sin i$ (km s ⁻¹)	4.5 ± 1	Thygesen et al. (2012)
log g (dex)	$2.89^{+0.19}_{-0.19}$	This work ^(a)
log g (dex)	2.776 ± 0.004	This work ^(b)
log g (dex)	2.80 ± 0.01	Thygesen et al. (2012)
log g (dex)	2.746 ± 0.067	Ghezzi & Johnson (2015) ^(c)
log g (dex)	2.800 ± 0.022	Ghezzi & Johnson (2015) ^(b)
log g (dex)	2.77 ± 0.01	Gaulme et al. (2020)
L (L_{\odot})	80.2 ± 9.5	This work
L (L_{\odot})	66.67	McDonald et al. (2012)
$\Delta\nu$ (μHz)	6.09 ± 0.07	This work
$\Delta\nu$ (μHz)	6.12 ± 0.12	Hekker et al. (2011)
$\Delta\nu$ (μHz)	6.18 ± 0.05	Gaulme et al. (2020)
ν_{max} (μHz)	70.4 ± 0.4	This work
ν_{max} (μHz)	76.00 ± 3.80	Hekker et al. (2011)
ν_{max} (μHz)	70.70 ± 0.45	Gaulme et al. (2020)
M_* (M_{\odot})	2.6 ± 0.1	This work
M_* (M_{\odot})	2.162 ± 0.236	Ghezzi & Johnson (2015) ^(c)
M_* (M_{\odot})	2.950 ± 0.504	Ghezzi & Johnson (2015) ^(b)
M_* (M_{\odot})	2.789 ± 0.139	Kervella et al. (2019)
M_* (M_{\odot})	2.14 ± 0.11	Gaulme et al. (2020)
R_* (R_{\odot})	11.2 ± 0.6	This work
R_* (R_{\odot})	9.996 ± 0.851	Ghezzi & Johnson (2015) ^(c)
R_* (R_{\odot})	11.255 ± 0.718	Ghezzi & Johnson (2015) ^(b)
R_* (R_{\odot})	10.686 ± 0.534	Kervella et al. (2019)
R_* (R_{\odot})	10.01 ± 0.21	Gaulme et al. (2020)
Age (Gyr)	8.64 ± 0.17	This work
Age (Gyr)	0.993 ± 0.298	Ghezzi & Johnson (2015) ^(c)
Status	He-core burning	This work
Status	RGB ^(d)	Thygesen et al. (2012)
Status	Red Clump	Gaulme et al. (2020)

Notes. ^(a)Spectroscopic analysis; ^(b)Asteroseismic analysis; ^(c)Evolutionary tracks; ^(d)Red giant branch star.

Gaia EDR3 data as 5.1501 ± 0.0597 mas (Gaia Collaboration 2016, 2021a), which implies an absolute magnitude $M_V = 0.69 \pm 0.03$ mag. Table 6 lists the stellar parameters known from the literature together with those determined in this work.

The basic stellar parameters were determined from a high-resolution ($R = 85\,000$) spectrum of HD 187878 taken with the HERMES spectrograph at the Mercator telescope with a S/N of ~ 160 . We followed the same procedure as in Sect. 3.1 on a wavelength range 4690–6700 Å, which provided the best results. The blue spectral range was omitted because of the presence of

dense molecular CNO lines that cannot be properly handled by SYNTHV (Tsymbal 1996).

Results of abundances of chemical elements are listed in Table 7. HD 187878 has a solar metallicity. We note that the abundances of C and N deviate from solar values, which confirms the trend of a nitrogen enrichment and a carbon deficiency in most giant stars as compared with main sequence stars (Kjaergaard et al. 1982).

The OCTAVE (Birmingham – Sheffield Hallam) automated pipeline (Hekker et al. 2010) was used to determine the large frequency separation between modes of consecutive order and the same degree, $\Delta\nu$, and the frequency of maximum oscillation power, ν_{max} . These values were combined in a grid-based modelling (Hekker et al. 2013) using T_{eff} and [Fe/H] from the spectroscopic measurements to determine the stellar mass, radius, age, and log g . All the resulting parameters are shown in Table 6.

4.2. Companion to HD 187878

We monitored HD 187878 for a time span of 12 years, during which we acquired 100 RV measurements (see Table 2 and Fig. 8). Our RV measurements show changes that could be caused by a low-mass stellar or a brown dwarf companion. As was done for KIC 3526061, we used the code PYANETI (Barragán et al. 2019) to find the orbital solution. We accounted for the RV zero points between the four different data sets with the advantage that data from different instruments have been taken close in time. The inferred parameters are given in Table 8. We also used FOTEL (Hadrava 2004) to independently check the orbital solution, and the resulting parameters were the same as with PYANETI within 1.5σ uncertainties. In Fig. 8 we show the RV measurements with the orbital solution and RV residuals with error bars after removing the orbital solution. Finally, the phase-folded RV variations for the orbital solution and the orbital fit are shown in Fig. 9. We also searched for additional periods in the residual RV data using the program PERIOD04 (Lenz & Breger 2005) and found a period of 194 d with a 3.0σ significance. As this period is very close to a half year and also has a low significance, we checked all individual data sets and found that this period is present only in the data from Ondřejov. Therefore, we searched in residual RV data again, but with the Ondřejov data excluded, and this time we did not find any significant periods (see Fig. 10).

4.2.1. Amplitude of stellar oscillations

The scatter of RV residuals after fitting the companion's orbit is 23.3 m s^{-1} . To estimate a velocity amplitude for stellar oscillations (Kjeldsen & Bedding 1995), we derived the stellar luminosity $L_* = 80.2 \pm 9.5 L_{\odot}$ using our estimated stellar effective temperature of $T_{\text{eff}} = 5168 \text{ K}$ and the stellar radius of $11.2 R_{\odot}$. We used this luminosity and our estimated stellar mass of $2.6 M_{\odot}$ to calculate a velocity amplitude of $\nu_{\text{osc}} = 7.2 \text{ m s}^{-1}$. We also used Eqs. (7) and (8) from Kjeldsen & Bedding (1995) to predict a velocity amplitude based on the luminosity amplitude from the Kepler light curves, and derived $\nu_{\text{osc}} = 1.7 \text{ m s}^{-1}$. The scatter of RV residuals is larger than both velocity amplitude estimates and is most likely due to uncertainties in RV measurements.

4.2.2. Orbital inclination and mass of a companion

Kervella et al. (2019) analysed the proper motion anomalies of nearby stars to characterise the presence of physical companions of stellar and sub-stellar mass. They used the HIPPARCOS

Table 7. Abundances of HD 187878 relative to solar composition.

C	N	O	Na	Mg	Si	Ca	Sc	Ti	V
$-0.24^{+0.10}_{-0.14}$	$+0.81^{+0.17}_{-0.24}$	$+0.10^{+0.44}_{-0.59}$	$+0.38^{+0.23}_{-0.26}$	$+0.18^{+0.12}_{-0.13}$	$-0.30^{+0.20}_{-0.24}$	$+0.07^{+0.26}_{-0.28}$	$+0.13^{+0.30}_{-0.38}$	$+0.13^{+0.11}_{-0.12}$	$+0.11^{+0.19}_{-0.21}$
Cr	Mn	Fe	Co	Ni	Y	Ba	Ce	Nd	Sm
$+0.06^{+0.13}_{-0.15}$	$+0.18^{+0.23}_{-0.26}$	$0.00^{+0.05}_{-0.05}$	$-0.04^{+0.17}_{-0.20}$	$-0.04^{+0.13}_{-0.14}$	$+0.08^{+0.41}_{-0.49}$	$+0.55^{+0.44}_{-0.81}$	$+0.18^{+0.32}_{-0.68}$	$+0.24^{+0.22}_{-0.27}$	$+0.20^{+0.39}_{-0.86}$

Table 8. Derived parameters of HD 187878 B.

Parameter	Value	Unit
Fitted		
Period	1452.3 ± 0.3	d
T_0	$2455\,836.0 \pm 0.4$	BJD
K	776.3 ± 1.6	m s^{-1}
e	0.342 ± 0.001	
ω	134.5 ± 0.2	deg
Derived		
$M \sin i$	78.4 ± 2.0	M_{Jup}
$T_{\text{periastron}}$	$2455\,923.1 \pm 0.9$	BJD
a	3.66 ± 0.08	AU
Other parameters		
$RV_0^{\text{Ondřejov}}$	16.4 ± 7.4	m s^{-1}
$RV_0^{\text{TLS old}}$	-78.2 ± 1.8	m s^{-1}
$RV_0^{\text{TLS new}}$	-42.8 ± 2.3	m s^{-1}
RV_0^{Mercator}	$-18\,285.3 \pm 0.6$	m s^{-1}
rms Total	23.3	m s^{-1}
rms Ondřejov	35.1	m s^{-1}
rms TLS old	17.0	m s^{-1}
rms TLS new	20.5	m s^{-1}
rms Mercator	19.4	m s^{-1}
Astrometry:		
Orbital inclination i	$9.8^{+0.4}_{-0.6}$	deg
Longitude of asc. node Ω	112 ± 2	deg
Correlation (i, Ω)	-0.35	
Mass M	535^{+44}_{-23}	M_{Jup}
Mass M	$0.51^{+0.04}_{-0.02}$	M_{\odot}

catalogue (van Leeuwen 2007) and *Gaia*'s second data release (Gaia Collaboration 2016, 2018) to determine the long-term proper motion of stars common to the two catalogues. They searched for a proper motion anomaly by comparing the long-term HiPPARCOS-*Gaia* and short-term *Gaia* proper motion vectors of each star, indicating the presence of a perturbing secondary object. Later, Kervella et al. (2022) used the *Gaia* EDR3 catalogue (Gaia Collaboration 2021a,b) and improved the accuracy of the detection of proper motion anomalies.

We used a combination of our spectroscopic orbital parameters presented in Table 8 and *Gaia* EDR3 astrometric proper motion anomaly (Kervella et al. 2022) to derive the orbital inclination and companion mass. We also used the HiPPARCOS proper motion anomaly (van Leeuwen 2007) to determine that the direction of the orbit is prograde. A more detailed description of the method can be found in Kervella et al. (2020). The inclination is found to be $i = 9.8^{+0.4}_{-0.6}$ deg which corresponds to the stellar companion's mass of $M = 535^{+44}_{-23} M_{\text{Jup}}$ or $0.51^{+0.04}_{-0.02} M_{\odot}$ (see Table 8). For this computation we adopted a stellar mass of $2.789 \pm 0.139 M_{\odot}$ (Kervella et al. 2019), and we also took into account the companion's mass and its eccentric orbit. The best-

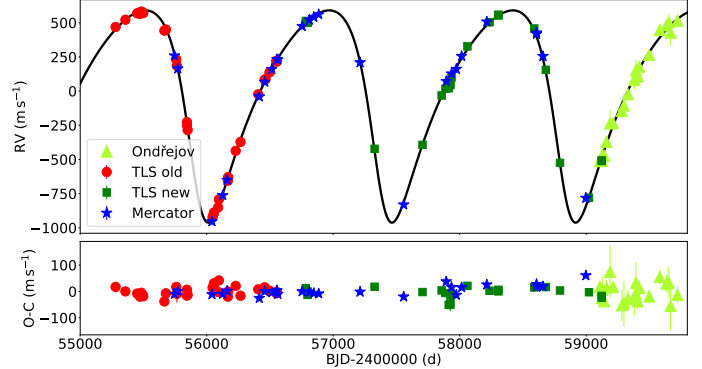


Fig. 8. Radial velocity measurements of HD 187878. *Top:* data obtained from March 2010 to May 2022 using the coude echelle spectrograph at TLS, Germany; the HERMES spectrograph at Mercator, La Palma; and the Ondřejov Echelle Spectrograph, Czech Republic. The solid curve represents the Keplerian orbital solution. *Bottom:* RV residuals and error bars after removing the orbital solution of HD 187878 B.

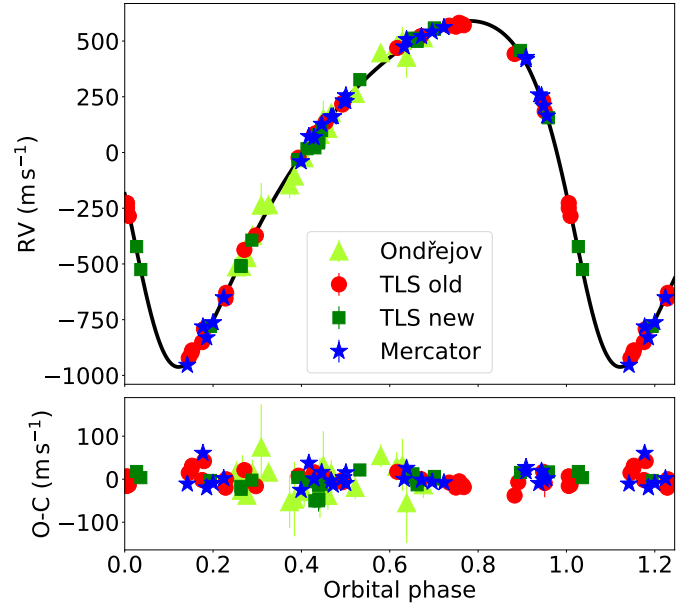


Fig. 9. Phased RV measurements of HD 187878. *Top:* data plotted with corresponding error bars and phased to the orbital period of 1452.3 d. The Keplerian orbital solution is overplotted with a solid curve. *Bottom:* RV residuals and error bars after removing the orbital solution of HD 187878 B.

fit orbit is displayed in Fig. 11. We note that the companion mass estimate in the catalogue of Kervella et al. (2022) is comparable to the value we obtain through a more refined analysis including the RVs.

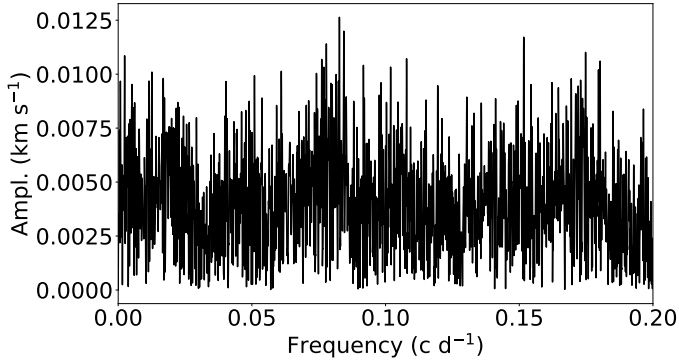


Fig. 10. Frequency amplitude spectrum of residual RV data of HD 187878 after removing the Keplerian orbital solution.

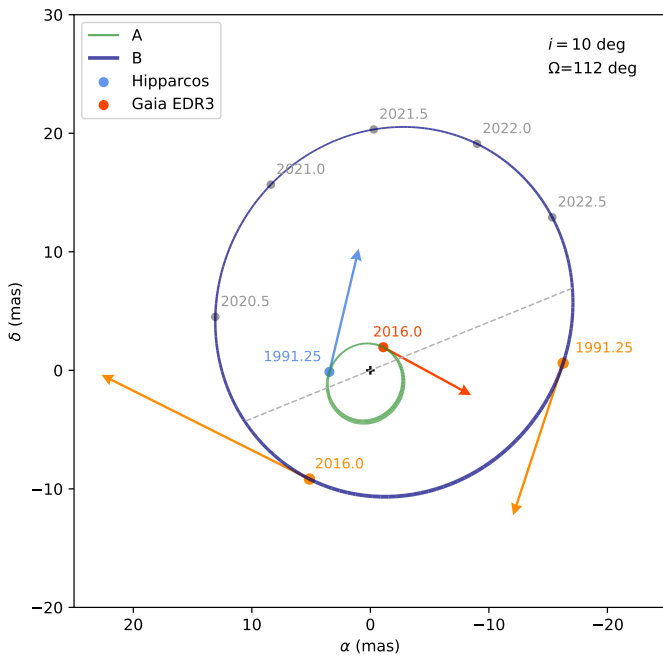


Fig. 11. Orbital trajectories of HD 187878 and HD 187878 B around their centre of mass. A thicker line indicates that the companion is closer to the Earth. The orange arrows show the velocity vector of HD 187878 B at the effective EDR3 and HIPPARCOS epochs. Although the HIPPARCOS proper motion anomaly vector is not fit, one can see that it is nicely tangent to the orbit.

4.3. Stellar activity analysis of HD 187878

4.3.1. Photometric variations

We analysed the *Kepler* photometry of HD 187878 as was done for KIC 3526061. The star was observed by the *Kepler* satellite (Borucki et al. 2010) starting in May 2009 and for all quarters during the main *Kepler* mission. The *Kepler* data have similar length to the orbital period of HD 187878 B. We do not find any long-term trends in the light curve. There is a feature around 600 Barycentric Kepler Julian Date (BKJD), which is most likely caused by an improper removal of systematic trends when creating PDCSAP light curves. Although the aperture for HD 187878 that was used to generate PDCSAP light curves contained several other stars with *Gaia* magnitudes $G = 14.1, 14.3, 15.5,$ and 16.8 , there is no obvious contamination of the flux of HD 187878, which has $G = 6.9$.

HD 187878 has also been observed in sectors 14 and 15 of the TESS satellite (Ricker et al. 2014). We used PDCSAP light curves, as above for the *Kepler* data, and found no long-term variations.

4.3.2. Stellar activity indicators

For the spectral line bisector analysis we proceeded as in Sect. 3.3.2 for the Mercator data. We measured the BVS of the spectral profile using the difference of the average bisector values between flux levels of 0.1–0.3 and 0.7–0.9 of the continuum value. A search for periods in the BVS variations using the program PERIOD04 (Lenz & Breger 2005) did not find any significant signal. The most significant frequency was found at the period of 328.5 d with a low 2.3σ significance.

As described in Sect. 3.3.3, we searched for periods in the FWHM variations and did not find any significant signal. The most significant frequency was found at the period of 556.1 d with a low 2.7σ significance.

We also analysed the chromospheric activity of HD 187878. In the Mercator data, first we removed telluric lines in the Ca II 8498 Å line. Then we measured the EQW at the central part of the Ca II 8498 Å line from 8497.45 to 8498.75 Å; of the Ca II 8542 Å line in the range ± 0.65 Å from the line centre; and of the Ca II 8662 Å line in two different ranges, 8661.6 to 8662.78 Å and 8661.1–8663.28 Å. For each spectrum, we made an average EQW based on the three Ca II lines and four different measurements, and finally searched for periods using the program PERIOD04 (Lenz & Breger 2005). The most significant frequency was found at the period of 4065 d with a low significance of 2.8σ . To summarise, we did not find any significant periods in any of the stellar activity indicators that were investigated.

5. Conclusions

We used precise stellar RV measurements of the intermediate-mass red giant branch star KIC 3526061 and the relatively massive, evolved red giant branch star HD 187878 to discover variations that we attribute to the presence of companions. We conclude that RV variations of KIC 3526061 are caused by a long-period eccentric companion that is very likely a brown dwarf, and that the RV variations of HD 187878 are due to a stellar companion.

For HD 187878 B we used a combination of spectroscopic orbital parameters and *Gaia* EDR3 astrometric proper motion anomaly (Kervella et al. 2022) to derive the orbital inclination and companion mass. We also used the HIPPARCOS proper motion anomaly (van Leeuwen 2007) to determine that the direction of the orbit is prograde. The inclination is found to be $i = 9.8^{+0.4}_{-0.6}$ deg, which corresponds to the companion’s mass in the stellar regime of $535^{+44}_{-23} M_{\text{Jup}}$ or $0.51^{+0.04}_{-0.02} M_{\odot}$.

KIC 3526061 b has a minimum mass $18.15 \pm 0.44 M_{\text{Jupiter}}$, but the unknown orbital inclination leaves an open question regarding the real nature of the companion. Under the assumption that inclination angles are randomly distributed on the sky, there is only a 2.6% chance for the companion mass to be greater than $80 M_{\text{Jupiter}}$, which is considered a dividing line between sub-stellar and stellar objects (Burrows et al. 2001; Hatzes & Rauer 2015; Chen & Kipping 2017). This means that most likely KIC 3526061 b is a sub-stellar object, either a brown dwarf or a giant planet.

The orbital period 3552^{+158}_{-135} d and orbital eccentricity 0.85 ± 0.01 makes KIC 3526061 b a unique sub-stellar companion

among those orbiting giant stars. It has the second largest eccentricity of sub-stellar companions orbiting giant stars. The origin of such a highly eccentric orbit is linked with the formation and dynamical history of KIC 3526061 b. Based on the population-level studies (Ma & Ge 2014; Nielsen et al. 2019; Wagner et al. 2019; Bowler et al. 2020) it seems more likely that KIC 3526061 b was formed via a gravitational instability. However, it cannot be excluded that KIC 3526061 b formed via a core accretion and developed such a large eccentricity through dynamical interactions with other companions. In addition, it is not clear whether population-level eccentricities of sub-stellar companions evolve over time or are established at young ages (Bowler et al. 2020). KIC 3526061 as the most evolved system found having a sub-stellar companion with such a large eccentricity and wide separation might provide a probe of the dynamical evolution of such systems over time.

In a spectral analysis of KIC 3526061 we encountered a large dependence between the projected rotational velocity $v \sin i$ and the macroturbulent velocity v_{macro} . This is not surprising since there is a tradeoff between $v \sin i$ and v_{macro} and a slight decrease in $v \sin i$ can be compensated for by an increase in v_{macro} . We analysed bisector velocity spans, a FWHM of spectral lines, and the EQW of the Ca II triplet lines and found stellar activity variations on a similar timescale of about 183 days in all three quantities. If these variations were related to a stellar rotation period of 183 days, then the projected rotational velocity would be $v \sin i = 1.6 \text{ km s}^{-1}$. However, we should be cautious as the signal is weak and has a period of about half a year. It is possible that the variations are due to changes in the instrumental profile, which is especially true of the McDonald data since there are moving components in the Tull spectrograph, such as the echelle grating and prisms, and they can be changed for different set-ups according to the observer's needs.

The search for potential transits of KIC 3526061 b is complicated by solar-like oscillations of KIC 3526061, which are larger than an expected transit depth and their variations have a timescale similar to the expected transit duration. In addition, unfortunately we do not have enough knowledge about potential transit times due to a large uncertainty in the orbital period. To refine the orbital solution more RV measurements from stable spectrographs are needed, and particularly observations around the time of the predicted periastron passage. Finally, given such a large orbital period of KIC 3526061 b, it shows the importance of having a long enough time series of observations in order to understand the occurrence of companions moving on long-period orbits.

Acknowledgements. Based on observations made with NASA's Discovery mission *Kepler* and with the HERMES spectrograph, installed at the *Mercator* telescope, operated on the island of La Palma by the Flemish Community, at the Spanish Observatorio del Roque de los Muchachos of the Instituto de Astrofísica de Canarias and supported by the Research Foundation – Flanders (FWO), Belgium, the Research Council of KU Leuven, Belgium, the Fonds National de la Recherche Scientifique (F.R.S.-FNRS), Belgium, the Royal Observatory of Belgium, the Observatoire de Genève, Switzerland and the Thüringer Landessternwarte Tautenburg, Germany. The data presented here have been taken using the 2 m *Alfred Jensch* Telescope of the Thüringer Landessternwarte Tautenburg, the 2.7 m *Harlan J. Smith* Telescope at the McDonald Observatory in Texas and at the 2 m *Perek* telescope at the Astronomical Institute of the Czech Academy of Sciences in Ondřejov. We are very grateful to the personnel of these facilities for their dedication and support during our observations. We thank our anonymous referee for giving us many useful suggestions for the improvement of the manuscript. This research has made use of the electronic bibliography maintained by NASA-ADS system and the SIMBAD data base, operated at CDS, Strasbourg, France. MK acknowledges the support from ESA-PRODEX PEA4000127913. RK, MS and PKa acknowledge the support by Inter-transfer grant no LTT-20015. AT acknowledges funding from the KU Leuven Research

Council (grant C16/18/005: PARADISE) and from the BELgian federal Science Policy Office (BELSPO) through PRODEX grant PLATO. We acknowledge the use of public TESS data from pipelines at the TESS Science Office and at the TESS Science Processing Operations Center. This work has made use of data from the European Space Agency (ESA) mission *Gaia* (<https://www.cosmos.esa.int/gaia>), processed by the Gaia Data Processing and Analysis Consortium (DPAC, <https://www.cosmos.esa.int/web/gaia/dpac/consortium>). Funding for the DPAC has been provided by national institutions, in particular the institutions participating in the Gaia Multilateral Agreement. This research made use of Lightcurve, a Python package for Kepler and TESS data analysis, and Astropy (<http://www.astropy.org>), a community-developed core Python package for Astronomy.

References

- Adamów, M., Niedzielski, A., Kowalik, K., et al. 2018, *A&A*, 613, A47
 Barragán, O., Gandolfi, D., & Antoniciello, G. 2019, *MNRAS*, 482, 1017
 Bergmann, C., Jones, M. I., Zhao, J., et al. 2021, *PASA*, 38, 15
 Borucki, W. J., Koch, D., Basri, G., et al. 2010, *Science*, 327, 977
 Boss, A. P. 1997, *Science*, 276, 1836
 Boss, A. P. 2006, *ApJ*, 643, 501
 Bowler, B. P., Johnson, J. A., Marcy, G. W., et al. 2010, *ApJ*, 709, 396
 Bowler, B. P., Blunt, S. C., & Nielsen, E. L. 2020, *AJ*, 159, 63
 Burrows, A., Hubbard, W. B., Lunine, J. I., & Liebert, J. 2001, *Rev. Mod. Phys.*, 73, 719
 Butler, R. P., Marcy, G. W., Williams, E., et al. 1996, *PASP*, 108, 500
 Chabrier, G., Johansen, A., Janson, M., & Rafikov, R. 2014, in *Protostars and Planets VI*, eds. H. Beuther, R. S. Klessen, C. P. Dullemond, & T. Henning, 619
 Chatterjee, S., Ford, E. B., Matsumura, S., & Rasio, F. A. 2008, *ApJ*, 686, 580
 Chen, J., & Kipping, D. 2017, *ApJ*, 834, 17
 Ciceri, S., Lillo-Box, J., Southworth, J., et al. 2015, *A&A*, 573, L5
 Cruzalèbes, P., Petrov, R. G., Robbe-Dubois, S., et al. 2019, *MNRAS*, 490, 3158
 De Ridder, J., Barban, C., Baudin, F., et al. 2009, *Nature*, 459, 398
 Elsworth, Y., Hekker, S., Basu, S., & Davies, G. R. 2017, *MNRAS*, 466, 3344
 Endl, M., Kürster, M., & Els, S. 2000, *A&A*, 362, 585
 Ford, E. B., & Rasio, F. A. 2008, *ApJ*, 686, 621
 Frandsen, S., Carrier, F., Aerts, C., et al. 2002, *A&A*, 394, L5
 Frink, S., Mitchell, D. S., Quirrenbach, A., et al. 2002, *ApJ*, 576, 478
 Gaia Collaboration (Prusti, T., et al.) 2016, *A&A*, 595, A1
 Gaia Collaboration (Brown, A. G. A., et al.) 2018, *A&A*, 616, A1
 Gaia Collaboration (Brown, A. G. A., et al.) 2021a, *A&A*, 649, A1
 Gaia Collaboration (Brown, A. G. A., et al.) 2021b, *A&A*, 650, C3
 Gaulme, P., Jackiewicz, J., Spada, F., et al. 2020, *A&A*, 639, A63
 Ghezzi, L., & Johnson, J. A. 2015, *ApJ*, 812, 96
 Ghezzi, L., Montet, B. T., & Johnson, J. A. 2018, *ApJ*, 860, 109
 Ginsburg, A., Sipőcz, B. M., Brasseur, C. E., et al. 2019, *AJ*, 157, 98
 Goldreich, P., & Sari, R. 2003, *ApJ*, 585, 1024
 Gray, D. F. 1988, *Lectures on spectral-line analysis: F, G, and K stars* (Arva: Ontario Gray)
 Grunblatt, S. K., Huber, D., Gaidos, E. J., et al. 2016, *AJ*, 152, 185
 Grunblatt, S. K., Huber, D., Gaidos, E., et al. 2017, *AJ*, 154, 254
 Grunblatt, S. K., Saunders, N., Sun, M., et al. 2022, *AJ*, 163, 120
 Hadrava, P. 2004, *Pub. Astron. Inst. Czech. Acad. Sci.*, 92, 1
 Hatzes, A. P., & Cochran, W. D. 1993, *ApJ*, 413, 339
 Hatzes, A. P., & Rauer, H. 2015, *ApJ*, 810, L25
 Hatzes, A. P., Cochran, W. D., Endl, M., et al. 2003, *ApJ*, 599, 1383
 Hatzes, A. P., Cochran, W. D., Endl, M., et al. 2015, *A&A*, 580, A31
 Hawkins, K., Masseron, T., Jofré, P., et al. 2016, *A&A*, 594, A43
 Hekker, S., Broomhall, A. M., Chaplin, W. J., et al. 2010, *MNRAS*, 402, 2049
 Hekker, S., Elsworth, Y., De Ridder, J., et al. 2011, *A&A*, 525, A131
 Hekker, S., Elsworth, Y., Mosser, B., et al. 2013, *A&A*, 556, A59
 Høg, E., Fabricius, C., Makarov, V. V., et al. 2000, *A&A*, 355, L27
 Hrudková, M., Hatzes, A., Karjalainen, R., et al. 2017, *MNRAS*, 464, 1018
 Huber, D., Bedding, T. R., Stello, D., et al. 2010, *ApJ*, 723, 1607
 Huber, D., Carter, J. A., Barbieri, M., et al. 2013, *Science*, 342, 331
 Huber, D., Zinn, J., Bojsen-Hansen, M., et al. 2017, *ApJ*, 844, 102
 Jofré, E., Almenara, J. M., Petrucci, R., et al. 2020, *A&A*, 634, A29
 Johnson, J. A., Aller, K. M., Howard, A. W., & Crepp, J. R. 2010, *PASP*, 122, 905
 Jones, M. I., Jenkins, J. S., Brahm, R., et al. 2016, *A&A*, 590, A38
 Jones, M. I., Brahm, R., Wittenmyer, R. A., et al. 2017, *A&A*, 602, A58
 Jorissen, A., Van Winckel, H., Siess, L., et al. 2020, *A&A*, 639, A7
 Kabáth, P., Skarka, M., Sabotta, S., et al. 2020, *PASP*, 132
 Kallinger, T., Mosser, B., Hekker, S., et al. 2010, *A&A*, 522, A1
 Kane, S. R., & von Braun, K. 2008, *ApJ*, 689, 492
 Kennedy, G. M., & Kenyon, S. J. 2008, *ApJ*, 673, 502

- Kervella, P., Arenou, F., Mignard, F., & Thévenin, F. 2019, *A&A*, **623**, A72
- Kervella, P., Arenou, F., & Schneider, J. 2020, *A&A*, **635**, L14
- Kervella, P., Arenou, F., & Thévenin, F. 2022, *A&A*, **657**, A7
- Kjaergaard, P., Gustafsson, B., Walker, G. A. H., & Hultqvist, L. 1982, *A&A*, **115**, 145
- Kjeldsen, H., & Bedding, T. R. 1995, *A&A*, **293**, 87
- Koubský, P., Mayer, P., Čáp, J., et al. 2004, *Pub. Astron. Inst. Czech. Acad. Sci.*, **92**, 37
- Kuschnig, R., Weiss, W. W., Gruber, R., Bely, P. Y., & Jenkner, H. 1997, *A&A*, **328**, 544
- Larson, A. M., Irwin, A. W., Yang, S. L. S., et al. 1993, *PASP*, **105**, 332
- Lee, B. C., Han, I., & Park, M. G. 2013, *A&A*, **549**, A2
- Lehmann, H., Tkachenko, A., Semaan, T., et al. 2011, *A&A*, **526**, A124
- Lenz, P., & Breger, M. 2005, *Commun. Asteroseismol.*, **146**, 53
- Lightcurve Collaboration (Cardoso, J. V. d. M., et al.) 2018, *Lightkurve: Kepler and TESS Time Series Analysis in Python*, Astrophysics Source Code Library [record ascl:1812.013]
- Lillo-Box, J., Barrado, D., Henning, T., et al. 2014, *A&A*, **568**, L1
- Linsky, J. L., Hunten, D. M., Sowell, R., Glackin, D. L., & Kelch, W. L. 1979, *ApJS*, **41**, 481
- Ma, B., & Ge, J. 2014, *MNRAS*, **439**, 2781
- Martínez Fiorenzano, A. F., Gratton, R. G., Desidera, S., Cosentino, R., & Endl, M. 2005, *A&A*, **442**, 775
- McDonald, I., Zijlstra, A. A., & Boyer, M. L. 2012, *MNRAS*, **427**, 343
- Mosser, B., Benomar, O., Belkacem, K., et al. 2014, *A&A*, **572**, L5
- Naoz, S. 2016, *ARA&A*, **54**, 441
- Ness, M., Hogg, D. W., Rix, H. W., et al. 2016, *ApJ*, **823**, 114
- Nielsen, E. L., Rosa, R. J. D., Macintosh, B., et al. 2019, *AJ*, **158**, 13
- Nowak, G., Niedzielski, A., Wolszczan, A., Adamów, M., & Maciejewski, G. 2013, *ApJ*, **770**, 53
- Ortiz, M., Gandolfi, D., Reffert, S., et al. 2015, *A&A*, **573**, L6
- Parker, R. J., Lichtenberg, T., & Quanz, S. P. 2017, *MNRAS*, **472**, L75
- Pasquini, L., Pallavicini, R., & Pakull, M. 1988, *A&A*, **191**, 253
- Pinsonneault, M. H., Elsworth, Y., Epstein, C., et al. 2014, *ApJS*, **215**, 19
- Pinsonneault, M. H., Elsworth, Y. P., Tayar, J., et al. 2018, *ApJS*, **239**, 32
- Pollack, J. B., Hubickyj, O., Bodenheimer, P., et al. 1996, *Icarus*, **124**, 62
- Quinn, S. N., White, T. R., Latham, D. W., et al. 2015, *ApJ*, **803**, 49
- Quirrenbach, A., Reffert, S., & Bergmann, C. 2011, *Am. Inst. Phys. Conf. Ser.*, **1331**, 102
- Raskin, G., van Winckel, H., Hensberge, H., et al. 2011, *A&A*, **526**, A69
- Reffert, S., Bergmann, C., Quirrenbach, A., Trifonov, T., & Künstler, A. 2015, *A&A*, **574**, A116
- Ricker, G. R., Winn, J. N., Vanderspek, R., et al. 2014, *SPIE Conf. Ser.*, **9143**, 914320
- Rodrigues, T. S., Girardi, L., Miglio, A., et al. 2014, *MNRAS*, **445**, 2758
- Sayed, M., Huber, D., Wheeler, A., & Ness, M. K. 2021, *AJ*, **161**, 170
- Silva Aguirre, V., Bojsen-Hansen, M., Slumstrup, D., et al. 2018, *MNRAS*, **475**, 5487
- Smith, J. C., Stumpe, M. C., Van Cleve, J. E., et al. 2012, *PASP*, **124**, 1000
- Stello, D., Huber, D., Bedding, T. R., et al. 2013, *ApJ*, **765**, L41
- Stumpe, M. C., Smith, J. C., Van Cleve, J. E., et al. 2012, *PASP*, **124**, 985
- The Astropy Collaboration (Price-Whelan, A. M., et al.) 2018, *AJ*, **156**, 123
- Thompson, S. E., Fraquelli, D., Van Cleve, J. E., & Caldwell, D. A. 2016, Kepler Archive Manual, Kepler Science Document KDMC-10008-006
- Thygesen, A. O., Frandsen, S., Bruntt, H., et al. 2012, *A&A*, **543**, A160
- Tkachenko, A. 2015, *A&A*, **581**, A129
- Tsymbal, V. 1996, *ASP Conf. Ser.*, **108**, 198
- Tull, R. G., MacQueen, P. J., Sneden, C., & Lambert, D. L. 1995, *PASP*, **107**, 251
- Valenti, J. A., Butler, R. P., & Marcy, G. W. 1995, *PASP*, **107**, 966
- van Leeuwen, F. 2007, *Hipparcos, the New Reduction of the Raw Data*, 350 (Springer Science+Business Media B.V.)
- Vrard, M., Kallinger, T., Mosser, B., et al. 2018, *A&A*, **616**, A94
- Wagner, K., Apai, D., & Kratter, K. M. 2019, *ApJ*, **877**, 46
- Wang, J., Shi, J., Pan, K., et al. 2016, *MNRAS*, **460**, 3179
- Wang, L., Sato, B., Omiya, M., et al. 2014, *PASJ*, **66**, 118
- Wenger, M., Ochsenbein, F., Egret, D., et al. 2000, *A&AS*, **143**, 9
- Whitworth, A. 2018, ArXiv e-prints [arXiv:1811.06833]
- Wittenmyer, R. A., Jones, M. I., Horner, J., et al. 2017, *AJ*, **154**, 274
- Yu, J., Huber, D., Bedding, T. R., et al. 2018, *ApJS*, **236**, 42
- Zechmeister, M., Köhler, J., & Chamathi, S. 2021, viper: Velocity and IP Estimator, Astrophysics Source Code Library [record ascl:2108.006]